Frequency Control for Improving Power Factor in Dynamic Wireless Power Transfer to Electric Vehicle

1st Yutaka Shikauchi
Graduate School of Frontier Sciences
The University of Tokyo
Chiba, Japan
shikauchi.yutaka22@ae.k.u-tokyo.ac.jp

2nd Kenichiro Takahashi
Honda R&D Co., Ltd.
Tochigi, Japan
kenichiro_takahashi@jp.honda

3rd Osamu Shimizu
Graduate School of Frontier Sciences
The University of Tokyo
Chiba, Japan
shimizu.osamu@k.u-tokyo.ac.jp

4th Hiroshi Fujimoto
Graduate School of Frontier Sciences
The University of Tokyo
Chiba, Japan
fujimoto@k.u-tokyo.ac.jp

***Abstract*—This paper focuses on changes in the phase difference of the transmitter side in wireless power transfer for electric vehicles, which are caused by variations in the receiver side voltage, resonance detuning, and mutual inductance. In particular, this study emphasizes the impact of changes in receiver side voltage. The slope and sign of the variation of the transmitter side phase difference with respect to the operating frequency are influenced by the receiver voltage. Additionally, the operating frequency at which the transmitter side phase difference becomes 0 differs, and maintaining a constant operating frequency can lead to the deterioration of the transmitter side power factor, increased switching losses, and reduced DC-to-DC efficiency. To address the degradation of the transmitter side phase difference caused by changes in the receiver side voltage, this paper discusses a method to improve the transmitter side power factor and reduce inverter losses through operating frequency control.**

***Index Terms*—Wireless power transfer, Electric vehicle, Receiver voltage, Power factor, Frequency control.**

I. Introduction

Wireless power transfer (WPT) for electric vehicles has garnered significant attention in recent years [1] - [6]. Dynamic wireless power transfer (DWPT) for electric vehicles (EV) is expected to extend their driving range and reduce the weight of onboard batteries. Consequently, international research utilizing actual vehicles is being conducted [7] - [9]. Additionally, companies have published papers focusing on the evaluation of leakage magnetic fields, with particular attention to high power transmitter and the scaling of coils [10], [11]. Furthermore, wireless power transfer in the MHz band is being conducted not only for EV but also for drones [12].

Wireless power transfer for electric vehicles, the power factor of the transmitter side inverter affects the electrical equipment capacity (kVA), DC-to-DC efficiency, and received power. These impacts are caused by increased switching losses and reactive power, prompting extensive research to address these issues [13] [14].

In study [13], research was conducted on maintaining constant transmitter side current amplitude, power factor, and received power by controlling the inverter's operating frequency, even when the coupling coefficient undergoes significant changes. This study demonstrated that by imposing constraints on the operating frequency control and the DC voltage ratio, the inverter's kVA can remain constant even with a 2.75-fold change in the coupling coefficient. Furthermore, in study [14], by designing the series resonance frequency according to a specific cost function, the range of coupling coefficients for which the inverter's kVA remains constant was improved by 50%. In these previous studies, the kVA remained constant in response to fluctuations in the coupling coefficient, enabling equipment minimization. However, these studies often referred to using the branched resonance frequency of the circuit, as discussed in parity time symmetry research [15] [16]. Therefore, constraints on the voltages at both sides are expected, and the AC-to-AC efficiency may be lower compared to when the central resonance frequency is used.

In this study, we investigate a method to always track the central resonance frequency, rather than the branched resonance frequency, for the operating frequency. In this approach, as the coupling coefficient decreases, the kVA is expected to increase. However, since voltage constraints are not required, this method is considered applicable to systems without a synchronous rectifier on the receiver side in the future. This study analyzes which parameters of the SS-type wireless power transfer system influence the central resonance frequency. Additionally, we clarify, through experiments and estimation, how the DC-to-DC efficiency and received power are affected when the operating frequency is fixed compared to when it is controlled to make the transmitter side phase difference 0 under conditions where the central resonance

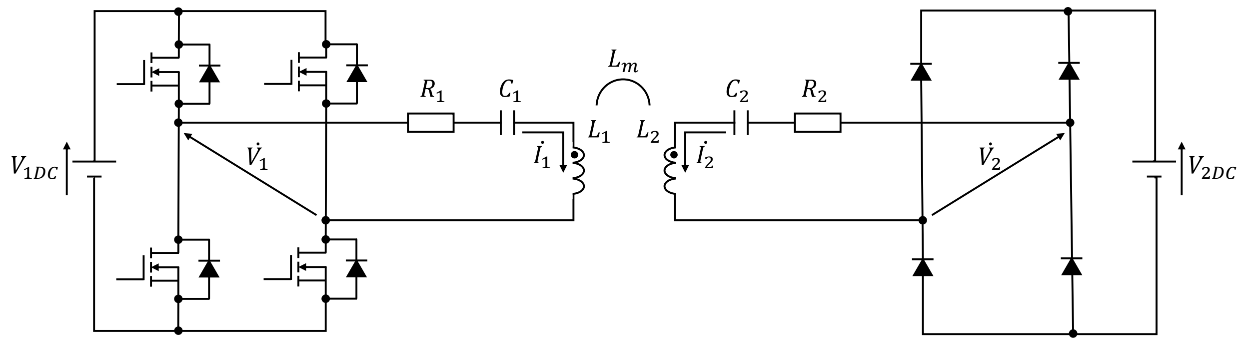

Fig. 1. Circuit model in SS-type.

TABLE I
ANALYSIS AND EXPERIMENTAL PARAMETERS.

Parameter	Symbol	Value
Transmitter DC voltage	V_{1DC}	150 V
Receiver DC voltage	V_{2DC}	75 V - 150 V
Self inductance of transmitter coil	L_1	55.3 µH
Self inductance of receiver coil	L_2	51.8 µH
Capacitor in transmitter side	C_1	66.2 nF
Capacitor in receiver side	C_2	71.5 nF
Winding resistance in transmitter side	R_1	131 mΩ
Winding resistance in receiver side	R_2	129 mΩ
Mutual inductance	L_m	10.5 µH

frequency changes.

II. Circuit Modeling

In this chapter, the circuit variables used in the analysis and experiments are explained. First, the circuit and its variables are described. Next, the resonant frequency of the circuit is derived from the introduced circuit variables.

A. Definition of Circuit Variables

Fig. 1. shows the WPT circuit using the SS method. In this circuit, the transmitter side is equipped with a full-bridge inverter, and the receiver side is equipped with a reactive diode rectifier circuit. In the circuit modeling, the components are considered ideal, neglecting the on-resistance and on-voltage of the transmitter side inverter and the receiver side diodes. In the variables, R represents the coil resistance, L represents the self-inductance of the coil, C represents the resonant capacitor, V represents the voltage, and I represents the current. The subscripts 1 and 2 indicate the transmitter side and receiver side, respectively. The dot above V and I represents the phasor. R_{Leq} represents the equivalent load resistance that simulates the battery load. L_m represents the mutual inductance between the transmitter side and the receiver side, and can be expressed using the coupling coefficient k as follows:

$$L_m = k\sqrt{L_1 L_2}. \tag{1}$$

Furthermore, the operating angular frequency ω_o and the series resonant angular frequencies ω_1 and ω_2 are defined as follows:

$$\omega_o = 2\pi f_o, \tag{2}$$

$$\omega_n = \frac{1}{\sqrt{L_n C_n}} = 2\pi f_n \quad n \in \{1, 2\}. \tag{3}$$

B. Circuit Resonant Frequency

The following circuit equations are used to derive expressions for $\dot{I}_1$ and $\dot{I}_2$.

$$\begin{bmatrix} \dot{V}_1 \\ 0 \end{bmatrix} = \begin{bmatrix} R_1 + j\omega_o L_1 \alpha & j\omega_o L_m \\ j\omega_o L_m & R_2 + R_{Leq} + j\omega_o L_2 \beta \end{bmatrix} \begin{bmatrix} \dot{I}_1 \\ \dot{I}_2 \end{bmatrix}, \tag{4}$$

$$\dot{I}_1 = \frac{(R_2 + R_{Leq} + j\omega_o L_2 \beta)\dot{V}_1}{(R_1 + j\omega_o L_1 \alpha)(R_2 + R_{Leq} + j\omega_o L_2 \beta) + \omega_o^2 L_m^2}, \tag{5}$$

$$\dot{I}_2 = \frac{-j\omega_o L_m \dot{V}_1}{(R_1 + j\omega_o L_1 \alpha)(R_2 + R_{Leq} + j\omega_o L_2 \beta) + \omega_o^2 L_m^2}. \tag{6}$$

The parameters α and β are defined as normalized quantities with respect to the frequency deviation ω_o from ω_1 and ω_2 as follows:

$$\alpha = 1 - \frac{\omega_1^2}{\omega_o^2}, \tag{7}$$

$$\beta = 1 - \frac{\omega_2^2}{\omega_o^2}. \tag{8}$$

Since R_{Leq} is not a fixed resistance load, it must be determined based on the magnitude ratio of $\dot{V}_2$ and $\dot{I}_2$. Here, we assume the approximations $R_1 \approx 0$ and $R_2 \approx 0$.

$$\begin{aligned} |R_{Leq}| &\approx \left| \frac{\dot{V}_2}{\dot{I}_2} \right| \\ &\approx \frac{\omega_o (L_m^2 - L_1 L_2 \alpha\beta)}{\sqrt{\left(\frac{V_1}{V_2}\right)^2 L_m^2 - L_1^2 \alpha^2}}. \end{aligned} \tag{9}$$

The phase difference of the transmitter side, θ_{Tx}, can be determined from $\dot{V}_1$ and $\dot{I}_1$ as follows:

$$\theta_{Tx} = \arctan\left(\frac{\mathrm{Im}\left[\frac{\dot{V}_1}{\dot{I}_1}\right]}{\mathrm{Re}\left[\frac{\dot{V}_1}{\dot{I}_1}\right]} \right). \tag{10}$$

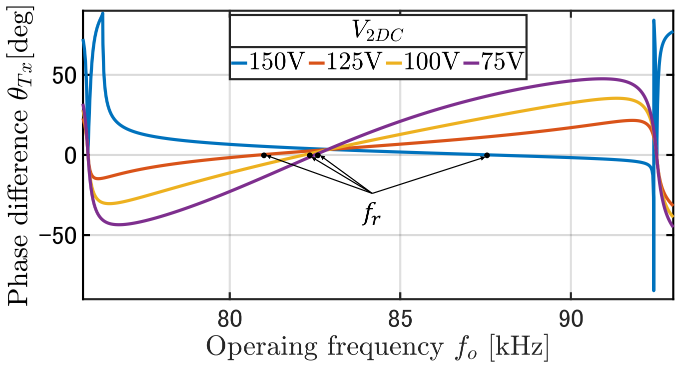

Fig. 2. Relationship between operating frequency and transmitter side phase difference (V_{1DC} = 150V).

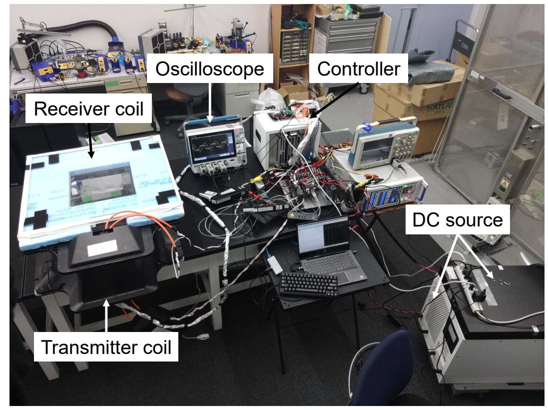

Fig. 3. Experiment Setup.

The resonance frequency of the circuit can be found by solving for ω_o such that $\theta_{Tx} = 0$, when $R_1 \approx 0$ and $R_2 \approx 0$. This gives the following equation:

$$\mathrm{Im}\left[\frac{\dot{V}_1}{\dot{I}_1}\right] = \omega_o L_1 \alpha - \frac{\omega_o^3 L_m^2 L_2 \beta}{(R_{Leq})^2 + (\omega_o L_2 \beta)^2} = 0. \tag{11}$$

Solving these equations yields the following expression:

$$(k^2 - \alpha\beta)\left[\alpha - \left(\frac{V_1}{V_2}\right)^2 \left(\frac{L_2}{L_1}\right)\beta\right] = 0. \tag{12}$$

The above equation suggests that the resonance frequency in the circuit shown in Fig. 1. depends on terms that vary with k, as well as terms that change with the voltages on the transmitter and receiver side and the self-inductances. In a static condition, factors other than the variation in k can affect the resonance frequency. However, under dynamic conditions, the resonance frequency is influenced by the k as well. In this study, it is assumed that V_2 varies depending on the vehicle, and thus $\alpha = \left(\frac{V_1}{V_2}\right)^2 \left(\frac{L_2}{L_1}\right)\beta$ is followed. Therefore, the target ω_o can be defined as ω_r and determined as follows:

$$\omega_r = \sqrt{\frac{\omega_1^2 - \frac{V_1^2}{V_2^2}\frac{L_2}{L_1}\omega_2^2}{1 - \frac{V_1^2}{V_2^2}\frac{L_2}{L_1}}} = 2\pi f_r. \tag{13}$$

III. Relationship between Operating Frequency and Transmitter Side phase difference

In this chapter, the relationship between f_o and θ_{Tx} is shown in the figure. Fig. 2. shows the relationship between f_o and θ_{Tx} when V_{2DC} changes. This analytical result is based on the parameters in Table 1. From this result, it can be inferred that the magnitude and sign of the slope of θ_{Tx} change with variations in V_{2DC}. In particular, the change in f_o where θ_{Tx} becomes 0 indicates that, without adjusting the operating frequency, it would lead to a deterioration in the transmitter side power factor and an increase in switching losses. Based on the analysis, it is necessary to actively adjust f_o, and particularly from the perspective of kVA, it is considered optimal to match f_r, the frequency at which the transmitter side power factor at θ_{Tx} = 0 becomes 1. Based on the above analytical results, the resonance frequency varies depending on the voltage conditions. In addition, as suggested by equation (13), it also changes with k, L_1 and L_2, indicating that it is necessary to actively adjust f_o even under dynamic conditions.

IV. Experiment

In this chapter, the experimental setup, comparison method, and experimental results are introduced.

A. Experiment Setup

The experimental environment used in this study is shown in Fig.3. In this setup, the transmitter coil and receiver coil are aligned for the experiment. The circuit is as shown in Fig.1. , and the experiment is conducted using a power supply simulating the transmitter side power source and another power supply simulating the receiver side battery. In the experimental results, an oscilloscope is used to display the waveforms of the transmitter side voltage and current, and a power meter is used to measure the losses and power factor.

B. Proposed Method and Comparison Method

In this study, the proposed method involves controlling the operating frequency to achieve θ_{Tx} = 0. This is because the central resonance frequency is influenced by V_{2DC}, and the goal is to follow this variation. The control method employs a hill climb approach, with the initial value of the operating frequency f_o set to 85 kHz, and the search begins from there. The control cycle is 5 µs. However, a comparison is made with the case where f_o is set to a constant 85 kHz.

The initial value of the operating frequency control is 85kHz in dynamic cindition, $V_{1DC} = 100\,\mathrm{V}$. PI controller is used for the frequency control. The P gain and I gain of the frequency control are 0.01 and 0.1, respectively. As a control structure, θ_{Tx} is feedbacked from the power transmitter side circuit. In addition, the difference compared to the command value $\theta_{Tx} = 0$ is input to the PI controller.

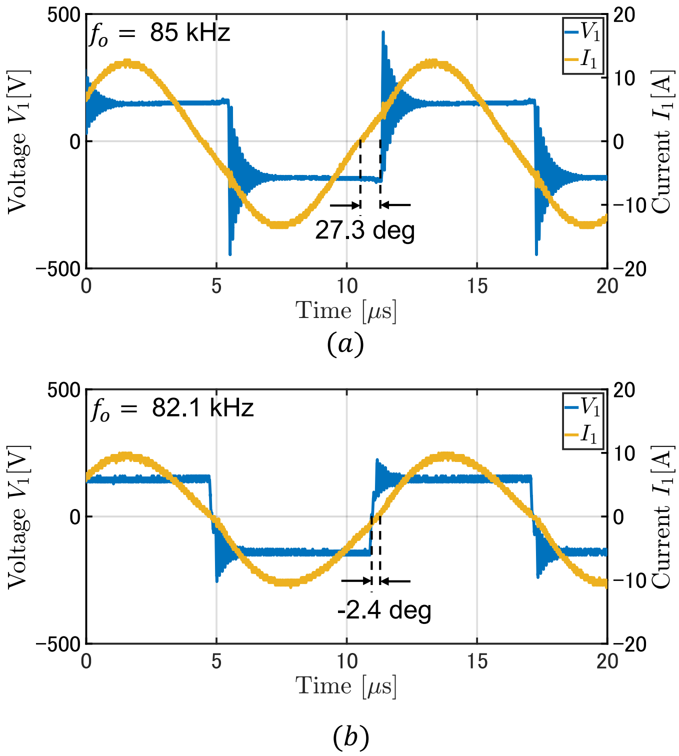

Fig. 4. Experimental waveforms with and without control (a) Without control (b) With control (V_{1DC} = 150V, V_{2DC} = 75V).

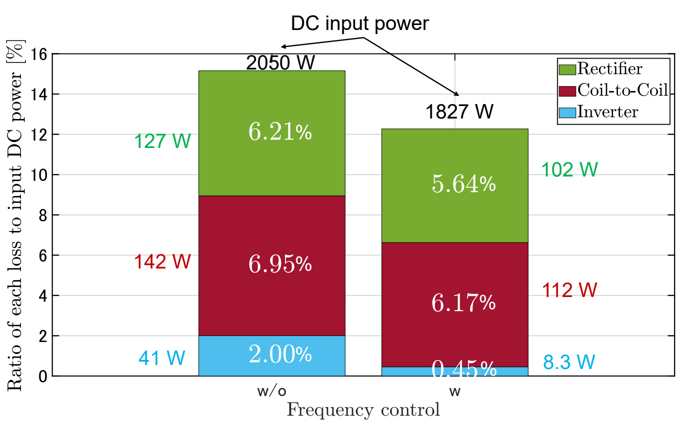

Fig. 5. Loss ratio of each part to input side DC power.

C. Experimental Results

1) Static Condition: Fig. 4. shows the waveforms of V_1 and I_1 when the operating frequency is not controlled and when it is controlled. In (a), the operating frequency is not controlled. The result shows that when f_o is 85 kHz, θ_{Tx} = 27.3 deg, and the transmitter side power factor is 0.889. In (b), the operating frequency is controlled so that the transmitter side power factor is 1. The result shows that when f_o is 82.1 kHz, θ_{Tx} = -2.4 deg, and the transmitter side power factor is 0.9991. From these results, it can be confirmed that the operating frequency control brings θ_{Tx} converge to 0, improving the power factor by 0.11.

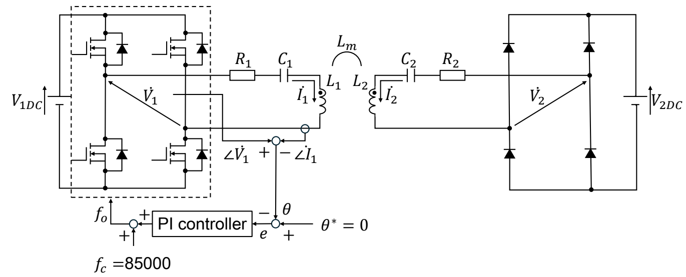

Fig. 6. Frequency control scheme in SS-type.

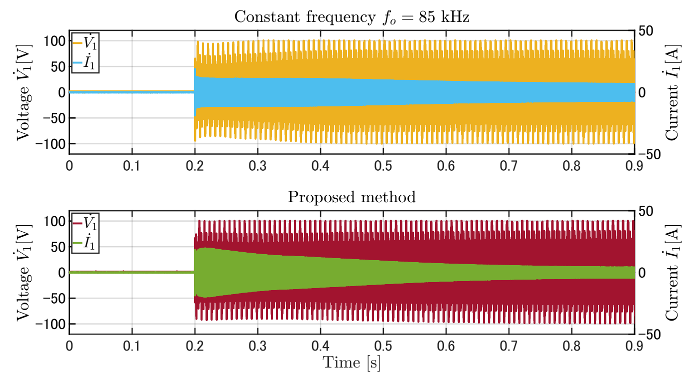

Fig. 7. Waveform of dynamic condition.

Fig. 5. shows the loss distribution of each component relative to the DC power on the transmitter side. Specifically, it shows the ratio of power consumed by the inverter, coil-to-coil (AC-to-AC), and rectifier to the DC power on the transmitter side. From these results, it can be seen that the proposed method reduces the power loss ratio in the inverter to 20%, suggesting that heat generation has been suppressed. Since the ringing of V_1 is smaller in (b), it can also be confirmed that the inverter's switching loss ratio has been reduced. The DC-to-DC efficiency was 0.848 in (a) and 0.878 in (b).

Based on the above results, an estimate of the received power P_o delivered to the vehicle side in (a) and (b) is performed. The estimation can be considered as the product of the inverter's kVA, the transmitter side power factor, and the DC-to-DC efficiency. For example, for a 10 kVA inverter, P_o is 7.5 kW in (a) and 8.7 kW in (b). Although this is an estimation, it can be concluded that improving the transmitter side power factor allows more power to be delivered to the vehicle side.

2) Dynamic condition: This chapter shows the effect of power factor improvement in DWPT. Fig. 6. shows the circuit structure and control configuration in dynamic condition. θ_{Tx} is feedback to control f_o through the PI controller. Then the nominal operating frequency f_c of 85 kHz is input in a feedforward. This control structure can adapt with changes in f_r due to voltage and resonance misalignment. Fig. 7. shows the results when f_o is kept constant and when the proposed method is applied and the power factor on the transmitter side is converge to 1. The waveforms are shown from the point

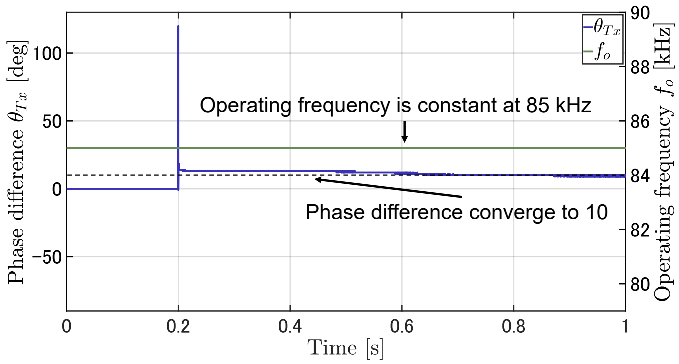

Fig. 8. Phase difference and operating frequency in constant frequency.

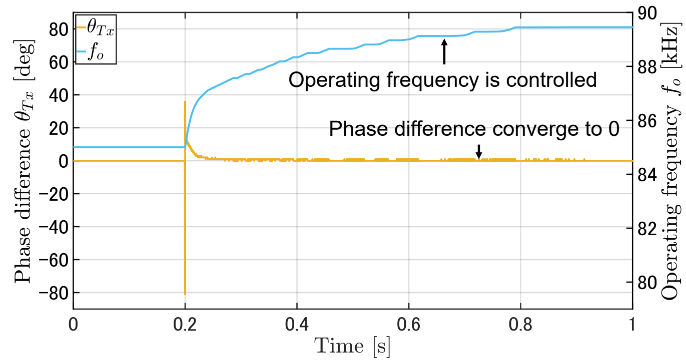

Fig. 9. phase difference and operating frequency in proposed method.

where the receiver coil approaches the transmitter coil and starts transmitter power until the receiver coil is directly above the transmitter coil.

The time variation of f_o and θ_{Tx} are shown in Figs. 8 and 9. In Fig. 8, f_o is constant at 85 kHz. Therefore, θ_{Tx} exceeds 10 deg. However, in Fig. 9, θ_{Tx} converges to 0 and the power factor converges to 1 because the operating frequency control is applied. If f_o is not varied as shown in Fig. 9, the transmitter side power factor never takes 1 when θ_{Tx} is 0. These would also vary depending on the battery voltage and manufacturing errors in the coils and capacitors of the resonant circuit.

Based on the above experimental results, it is possible to achieve a transmitter side power factor of 1 in both static and dynamic conditions by controlling the operating frequency. However, since the steady-state current tends to increase under low coupling conditions, future work will consider suppressing this in order to reduce the required kVA capacity of the inverter.

V. Conclusion

This paper presents a study on wireless power transfer for electric vehicles. In particular, it focuses on the scenario in which vehicles with different receiver side voltages enter the system while the transmitter side voltage is kept constant. This causes a change in the transmitter side phase difference and deterioration of the transmitter side power factor. The analysis revealed that as the ratio between the transmitter side and receiver side voltages and coupling coefficient changes, the transmitter side phase difference also changes in relation to the operating frequency. In the proposed method, by tracking the central resonance point of the circuit, it was confirmed that the transmitter side power factor and DC-to-DC efficiency are superior compared to when the operating frequency is kept constant. Additionally, rough calculations suggested that for an inverter with the same electrical capacity, controlling the operating frequency allows more power to be transmitted to the vehicle side. The results under dynamic conditions also showed that it is possible to control the transmitter side power factor to 1 even under dynamic conditions. These results suggest that reactive power is reduced. These results suggest that the electrical capacity of the inverter can be effectively utilized. Future work will include quantitative comparisons with previous studies and analysis of gain and stability in operating frequency control.

Acknowledgment

This work was supported by Council for Science, Technology and Innovation(CSTI), Cross-ministerial Strategic Innovation Promotion Program (SIP), the 3rd period of SIP " Smart energy management system "Grant Number JPJ012207 (Funding agency:JST).

References

[1] Y. Li, S. Wang, Y. Wu, Y. Jiang, Z. Xiao and Y. Tang, "Heterogeneous Integration of Isotropic and Anisotropic Magnetic Cores for Inductive Power Transfer," in IEEE Transactions on Power Electronics, vol. 40, no. 2, pp. 3770-3784, Feb. 2025.

[2] H. Zhang, F. Lu and C. Mi, "An Electric Roadway System Leveraging Dynamic Capacitive Wireless Charging: Furthering the Continuous Charging of Electric Vehicles," in IEEE Electrification Magazine, vol. 8, no. 2, pp. 52-60, June 2020.

[3] J. Wu, H. Yuan, S. Li, S. -C. Tan and S. -Y. R. Hui, "A Novel Scheme with Maximum Efficiency and Fast Response for Dynamic Wireless Battery Charging Systems," 2024 IEEE Energy Conversion Congress and Exposition (ECCE), Phoenix, AZ, USA, 2024, pp. 2067-2071.

[4] A. Zahid, M. Hansen, M. Chawla, A. Kamineni and R. A. Zane, "Robust Communicationless Control Strategy to Synchronize In-Motion Secondary to the Primary," 2024 IEEE Wireless Power Technology Conference and Expo (WPTCE), Kyoto, Japan, 2024, pp. 576-581.

[5] S. Cruciani, T. Campi, F. Maradei and M. Feliziani, "Active Shielding Design for a Dynamic Wireless Power Transfer System," 2020 International Symposium on Electromagnetic Compatibility - EMC EUROPE, Rome, Italy, 2020, pp. 1-4.

[6] Daisuke Gunji, Osamu Shimizu, Sakahisa Nagai, Toshiyuki Fujita, Hiroshi Fujimoto, Greenhouse Gas Emission Evaluation Including Infrastructure for Passenger Electric Vehicles with Dynamic Wireless Power Transfer, IEEJ Journal of Industry Applications, March 2025.

[7] A. N. Azad, A. Echols, V. A. Kulyukin, R. Zane and Z. Pantic, "Analysis, Optimization, and Demonstration of a Vehicular Detection System Intended for Dynamic Wireless Charging Applications," in IEEE Transactions on Transportation Electrification, vol. 5, no. 1, pp. 147-161, March 2019.

[8] Z. Deng et al., "Design of a 60-kW EV Dynamic Wireless Power Transfer System With Dual Transmitters and Dual receivers," in IEEE Journal of Emerging and Selected Topics in Power Electronics, vol. 12, no. 1, pp. 316-327, Feb. 2024.

[9] T. Koishi, B. -M. Nguyen, O. Shimizu and H. Fujimoto, "Receiving Side Current-Based Lateral Misalignment Estimation and Automated Steering Control for Dynamic Wireless Power Transfer," in IEEE Journal of Emerging and Selected Topics in Industrial Electronics, vol. 6, no. 1, pp. 41-52, Jan. 2025.

[10] Jin Katsuya, Shuji Kawano, Kenichiro Takahashi, 150kW Dynamic Wireless Power Transfer Inverter Control Technology, Transactions of Society of Automotive Engineers of Japan, 2023-2024, Volume 55, Issue 5, Pages 942-947, 2024 (Japanese).

[11] Sumiya, Hayato & Takahashi, Eisuke & Yamaguchi, Nobuhisa & Tani, Keisuke & Nagai, Sakahisa & Fujita, Toshiyuki & Fujimoto, Hiroshi, "Coil Scaling Law of Wireless Power Transfer Systems for Electromagnetic Field Leakage Evaluation for Electric Vehicles", IEEJ Journal of Industry Applications, 2021.

[12] L. Lan, C. H. Kwan, J. M. Arteaga, D. C. Yates and P. D. Mitcheson, "A 100W 6.78MHz Inductive Power Transfer System for Drones," 2020 14th European Conference on Antennas and Propagation (EuCAP), Copenhagen, Denmark, 2020, pp. 1-4.

[13] G. Guidi and J. A. Suul, "Minimizing Converter Requirements of Inductive Power Transfer Systems With Constant Voltage Load and Variable Coupling Conditions," in IEEE Transactions on Industrial Electronics, vol. 63, no. 11, pp. 6835-6844, Nov. 2016.

[14] Andrey Vulfovich, Alon Kuperman, Extending the design space of minimized VA rating inductive wireless power transfer links operating in restricted sub-resonant frequency region with constant current output, Energy, Volume 310, 2024.

[15] J. Zhou, B. Zhang, G. Liu and D. Qiu, "Resonance and Distance Insensitive Wireless Power. Transfer with Parity-Time Symmetric Duffing Resonators," 2018 IEEE Wireless Power Transfer Conference (WPTC), Montreal, QC, Canada, 2018, pp. 1-4.

[16] Toshiyuki Fujita, Kodai Takeda, Takehiro Imura, Takafumi Koseki, Yusuke Minagawa,Interoperability Verification of Wireless Power Transfer System with Separate Reference Impedance Map Method,IEEJ Journal of Industry Applications, Vol. 13, No. 5, pp.530-538, 2024.